

See discussions, stats, and author profiles for this publication at: <https://www.researchgate.net/publication/282852881>

Luminescent Copper Nanoclusters as a Specific Cell-Imaging Probe and a Selective Metal Ion Sensor

ARTICLE in THE JOURNAL OF PHYSICAL CHEMISTRY C · OCTOBER 2015

Impact Factor: 4.77 · DOI: 10.1021/acs.jpcc.5b08123

CITATION

1

READS

26

5 AUTHORS, INCLUDING:



Nirmal Kumar Das

Indian Institute of Science Education and Res...

6 PUBLICATIONS 7 CITATIONS

[SEE PROFILE](#)



Subhadip Ghosh

Indian Institute of Science Education and Res...

12 PUBLICATIONS 57 CITATIONS

[SEE PROFILE](#)



Amulya Priya

Indian Institute of Science Education and Res...

4 PUBLICATIONS 10 CITATIONS

[SEE PROFILE](#)



Saptarshi Mukherjee

Indian Institute of Science Education and Res...

49 PUBLICATIONS 639 CITATIONS

[SEE PROFILE](#)

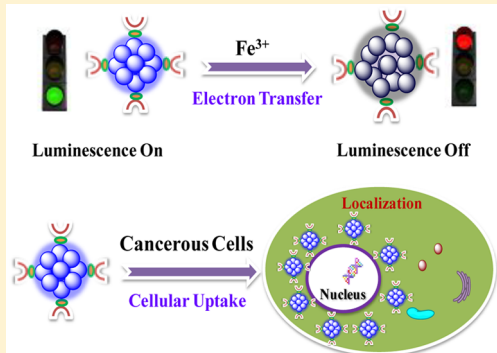
Luminescent Copper Nanoclusters as a Specific Cell-Imaging Probe and a Selective Metal Ion Sensor

Nirmal Kumar Das,[†] Subhadip Ghosh,[†] Amulya Priya,[‡] Sunando Datta,[‡] and Saptarshi Mukherjee*,[†]

[†]Department of Chemistry, and [‡]Department of Biological Sciences, Indian Institute of Science Education and Research Bhopal, Bhopal Bypass Road, Bhauri, Bhopal 462 066, Madhya Pradesh, India

 Supporting Information

ABSTRACT: Copper nanoclusters (CuNCs) exhibit a high tendency to undergo oxidation particularly at the subnanometer size regime. In the light of overcoming this bottleneck, we have been successful in developing tripeptide (glutathione, GSH) templated CuNCs which show high biocompatibility and stability, in spite of being ultrafine in size. These blue-emitting CuNCs possess very promising optical features such as significant quantum yield (QY) and excellent photostability. Our cell-imaging studies reveal that the CuNCs localize primarily in nuclear membranes of the different cancerous (HeLa, MDAMB-231, and A549) cells, and the cell viability assay conclusively established their nontoxic nature. Apart from their biological significances, these CuNCs also illustrate their ability to serve as a metal ion sensor, selectively detecting Fe^{3+} ions in solution at the nanomolar concentration regime. This unique luminescent property of the NCs will enable them to serve as label-free and versatile probes having several biological and analytical applications.



1. INTRODUCTION

Metal nanoclusters (NCs) have emerged as a supreme class of materials in the modern development of nanosciences and nanotechnology possessing some superior optical characteristics in terms of their high photostability, quantum yield (QY), biocompatibility, and water solubility.^{1–3} The ultrasmall size regime of these NCs (<1 nm, comparable to the Fermi wavelength of conduction electrons) results in its quantum-like behavior giving rise to discrete electronic transitions and size-dependent luminescence, in contrast to metal nanoparticles which are larger in size.^{3,4} Further, these NCs are less toxic than quantum dots which closely resemble them in terms of quantum phenomenon.^{4,5}

Several synthetic strategies have been proposed for these NCs using various self-organized assemblies, like protein,³ DNA,⁶ peptides,⁷ polymer,⁸ dendrimer,⁹ and thiols^{1,10} as templates. As the synthetic protocol of NCs mentioned herein is biocompatible and nontoxic, hence it can be efficiently applied for cell imaging, optical sensing, and various biomedical investigations.³ During the past decade researchers mainly focused on the synthesis of gold and silver NCs and developed multiple interdisciplinary applications using them as the luminescent probes.¹¹ On the contrary, copper NCs (CuNCs) are still rarely explored due to the limitations involved in their synthesis in controlling ultrafine size and their propensity to undergo oxidation.^{11–14} Among different templates used for the synthesis of NCs, the small thiol group occupies a seminal position due to its enhanced chemical stability, ultrafine size, and tailororable surface properties.¹² However, there are very few reports in the literature on the

synthesis of thiolate (like glutathione, GSH) protected CuNCs.^{1,15} Hence, development of synthetic protocol for monodispersed, nontoxic, chemical, and photostable thiol-protected CuNCs has always been a challenge for researchers. These CuNCs are extremely versatile and have a broad range of applications from biomedical probes, to photocatalysis, to light harvesting devices.^{10,14,16}

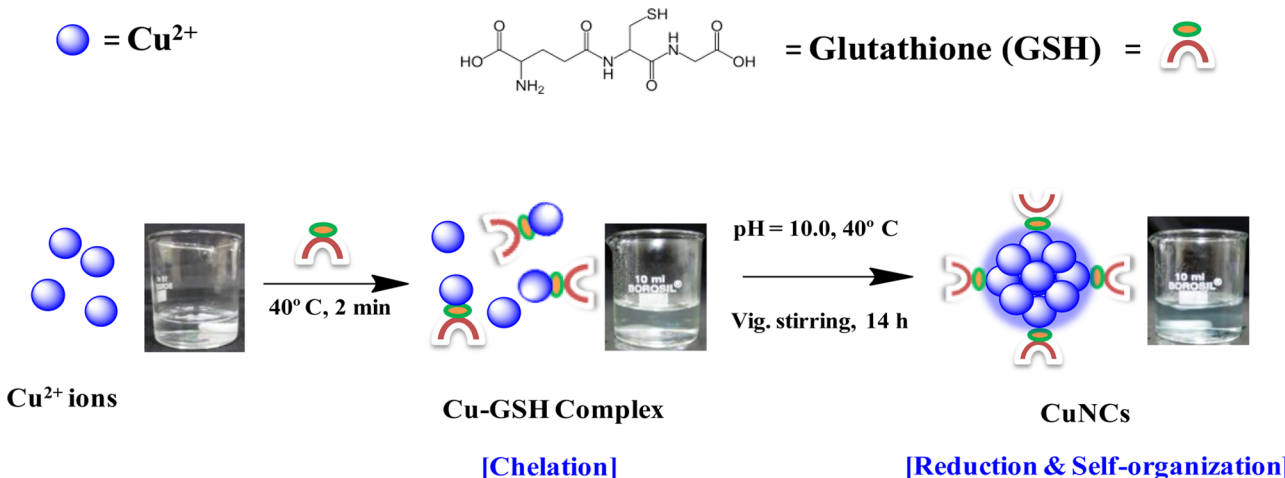
Monitoring the subcellular region using the fluorescence imaging technique is really important in clinical technology.^{17,18} Nontoxic NCs have great advantage to resolve these challenges. Also, detection of biologically significant metal ions in the nanomolar concentration regime has immense importance in analytical studies.^{19,20} Among several metals, iron plays a frontier role in biological systems like enzyme activity, electron transfer, metabolism, etc.^{21,22} The ferrous/ferric [Fe(II)/Fe(III)] system is the major redox pair in the electron transport of the respiratory panels.^{19,21,22} The deviation from the uniform balance of Fe in physiological systems leads to many serious diseases,²² and hence, its quantification in the biological system is of utmost importance.²³

In this communication, we report for the first time, a very efficient protocol for synthesizing blue-emitting luminescent CuNCs using GSH as a protecting group as well as reducing agent. For characterizing these ultrasmall monodispersed NCs, we used matrix-assisted laser desorption ionization time-of-flight (MALDI-TOF) mass spectrometric and transmission

Received: August 20, 2015

Revised: October 3, 2015

Scheme 1. Schematic Representation of Formation of the Blue-Emitting CuNCs Using GSH as Template as Well as Reducing Agent along with Their Corresponding Photographic Images



electron microscopy (TEM) analysis. The synthesized CuNCs exhibited good photostability, high QY (~6%), and luminescent lifetime of ~2.72 ns. Besides serving as potential probes for primarily marking the nuclear membrane of the different cancerous cells, our synthesized CuNCs displayed potential as metal ion sensors, as they detected Fe^{3+} ions selectively at nanomolar concentration in solution.

2. EXPERIMENTAL SECTION

2.1. Materials. Glutathione, copper nitrate [$\text{Cu}(\text{NO}_3)_2$], sodium hydroxide (NaOH), rhodamine B, coumarin-153, human hemoglobin (Hb), $\text{K}_2\text{Cr}_2\text{O}_7$ and the chlorides of other metals were all purchased from Sigma-Aldrich and were used as received. Dulbecco's modified Eagle's medium (DMEM), F12K medium, L15 medium, fetal bovine serum (FBS), 100 $\mu\text{g}/\text{mL}$ penicillin, 100 $\mu\text{g}/\text{mL}$ streptomycin and glutamine, CellTracker Green CMFDA, and trypan blue reagents were all purchased from Life Technologies. Milli-Q water was used to prepare solutions throughout the experiments.

2.2. Instrumentation. Steady-state absorption measurements were carried out in a Carry-100 UV-vis spectrophotometer by scanning in the range from 200 to 600 nm. Steady-state luminescence data were recorded on a Horiba Jobin-Yvon, Fluorolog 3-111. The luminescence spectra were measured with a 2 mm path length quartz cuvette. The CuNCs were excited at 340 nm, and emission was collected from 355 to 650 nm with an integration time of 0.1 s. The emission and the excitation slits both were kept at 5 nm. For lifetime measurements, the CuNCs were excited at 340 nm using an IBH-NanoLED source N-340, a picosecond diode. The emission was collected at magic angle polarization using a Hamamatsu MCP photomultiplier (model R-3809U-50). The time-correlated single-photon counting (TCSPC) setup consisted of an Ortec 9327 pico-timing amplifier. The data was collected with a PCI-6602 interface card as a multichannel analyzer. The full width at half-maximum (fwhm) of the system response was about 750 ps.

MALDI-TOF mass spectrometry studies were carried out using Bruker Daltonics UltraflexXtreme MALDI-TOF/TOF in the positive ion mode and 2,5-dihydroxybenzoic acid as the matrix. A Zeiss confocal laser scanning microscope has been used for the imaging studies using a 488 nm laser source. TEM

images were obtained from a JEOL JEM 2100 F (field emission electron microscope) operating at 200 kV. Carbon-coated Cu grids were used for sample preparation.

2.3. Metal Ion Sensing Procedure. The salts of metal ions Na^+ , Mg^{2+} , Ca^{2+} , K^+ , Mn^{2+} , Cr^{6+} , Fe^{3+} , Co^{2+} , Ni^{2+} , Cu^{2+} , Zn^{2+} , Hg^{2+} , and Pb^{2+} were taken, and their aqueous solutions were prepared in Milli-Q water in higher concentrations. These solutions were further diluted, and microliter aliquots of the respected diluted solutions of the metal ions were added to 0.6 mL of a solution of the NCs in such a way that the desired final concentration of metal ion(s) in the solution is achieved. The solutions were made homogeneous by thorough mixing and were then incubated at room temperature for 3 min. Subsequently, they were transferred into the cuvette and the corresponding luminescences were recorded. The limit of detection (LOD) was calculated from the luminescence intensity, where the change in luminescence intensity in the presence of Fe^{3+} ions was above 3 times the standard deviation for CuNCs in the absence of any Fe^{3+} ions.²⁰

2.4. Cell Imaging and Cell Viability Assay. 2.4.1. *Cell Culture.* Hela cells were cultured at 37 °C with 5% CO₂ in DMEM supplemented with 10% FBS, 100 µg/mL penicillin, 100 µg/mL streptomycin, and 2 mM glutamine. MDAMB-231 cells were cultured at 37 °C without CO₂ in L15 medium supplemented with 10% FBS, 100 µg/mL penicillin, and 100 µg/mL streptomycin. A549 cells were cultured at 37 °C with 5% CO₂ in F12K medium supplemented with 10% FBS, 100 µg/mL penicillin, and 100 µg/mL streptomycin. Cell viability and uptake assays were performed in a 24-well plate, where cells ($n = 25\,000$) were grown on coverslips 1 day prior to the experiment.

2.4.2. Uptake Assay of CuNCs in Different Cancerous Cells and Cell Viability Test. Cells were grown on coverslips in 24-well plates. Cells were incubated for different time points (2, 4, 6, 8, 15, and 36 h) with varying concentrations of the NCs (0.1, 1, 5, 10, 20, 30, 100, 150, and 200 μ M) as shown in Table S1. The viability of the cells was checked after each time point by observation under the microscope using trypan blue staining. This method is based on the principle that live (viable) cells do not take up certain dyes, whereas dead (nonviable) cells do. Staining facilitates the visualization of cell morphology. The same procedure was followed for all three different cell lines.

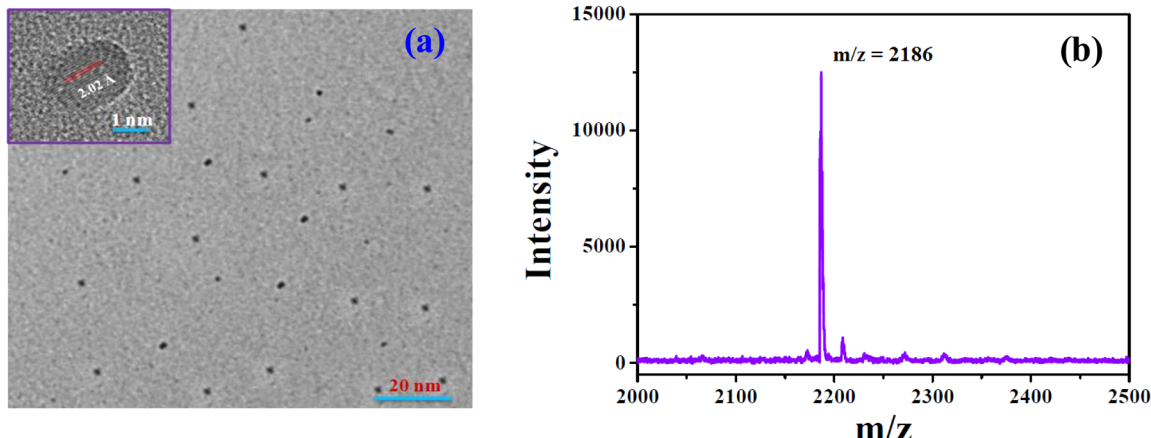


Figure 1. (a) TEM image of the CuNCs. The inset shows the image of a single NC exhibiting lattice fringes. (b) MALDI-TOF spectrum of the monodispersed CuNCs. A single base peak has been obtained at $m/z = 2186$ Da.

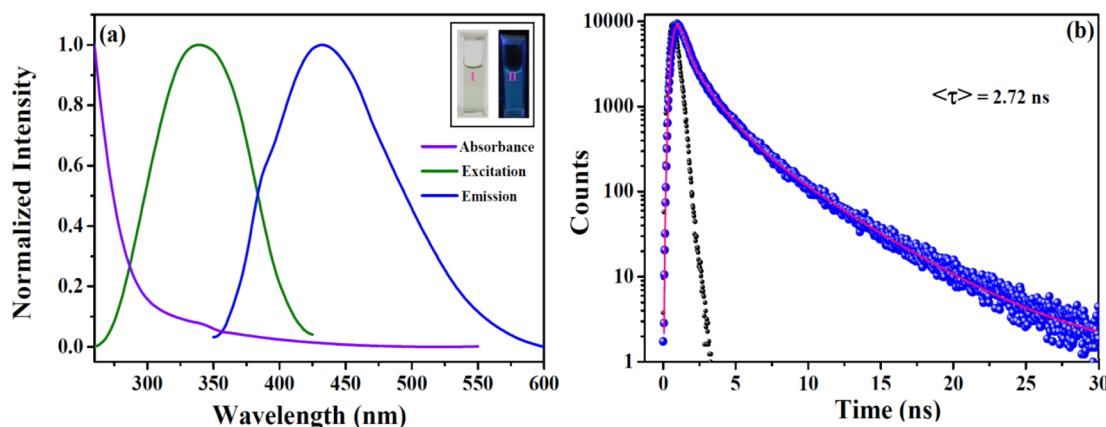


Figure 2. (a) Normalized absorption, excitation, and emission spectra of the CuNCs as marked in the figure. The inset shows the photographic images of the CuNCs under (I) visible light and (II) UV light. (b) Representative lifetime decay profile (in logarithmic scale) of the CuNCs.

2.4.3. CellTracker Green Staining. CellTracker Green CMFDA was dissolved in DMSO to prepare a 10 mM stock solution. A 5 μ M staining solution in serum-free DMEM was prepared. The adherent cells were washed twice with phosphate buffer saline (PBS), pH 7.4. The cells were incubated at 37 °C with 5 μ M staining solution for 30 min. The staining solution was replaced with serum-free media, and the mixture was incubated for 30 min at 37 °C. The cells were again washed with PBS and preceded for microscopy-based localization studies.

2.4.4. Subcellular Localization. Before fixation, cells were washed twice with PBS. Cells were fixed in 4% paraformaldehyde for 15 min at room temperature. After fixation cells were again washed twice with PBS and finally with water before mounting on glass slides. The coverslips were mounted using Mowiol on glass slides, and images were acquired using a Zeiss confocal microscope.

3. RESULTS AND DISCUSSION

3.1. Synthetic Protocol and Subsequent Characterizations of the CuNCs. Availability of the thiol group in GSH is facilitating the metal–ligand chelation which is further ensuring the formation of the CuNCs. The typical synthetic procedure involves mixing of optimized concentration of $\text{Cu}(\text{NO}_3)_2$ (5 mM) to GSH solution (5 mM) under vigorous stirring followed by the addition of NaOH to the maintain a pH

of ~10. The mixture was incubated at 40 °C for 14 h under constant vigorous stirring to obtain a light green solution. (Please refer to the Supporting Information for details of synthetic protocol and optimization process, Figures S1–S3.) The probable mechanism of the formation of CuNCs is as underlined: initially metal–ligand chelate formation takes place where the Cu^{2+} ions coordinate and get electrostatically stabilized by both thiol as well as carboxylate groups of GSH, strongly resembling the process of biominerization³ (Scheme 1). Here, GSH plays a dual role of being a stabilizing agent and a reductant.

Further addition of NaOH (pH ~ 10) enhances the reducing capability of the –SH group ($pK_a \sim 9.35$),²⁴ thereby reducing the Cu ions to atoms, and induces a coalescence process which ultimately leads to the formation of stable CuNCs. To the best of our knowledge, we are reporting for the first time a biocompatible one-pot synthesis of blue-emitting CuNCs using GSH as a template.

TEM analysis revealed the existence of the spherical NCs with a size regime ~2.2 nm which also exhibits crystal lattice fringes (Figure 1a). The exact atomic composition (number of Cu atoms and GSH molecules) comprising the CuNCs was determined using MALDI-TOF mass spectrometric analyses. From the mass data, the base peak is centered at $m/z = 2186$. Taking the molecular weight of GSH and atomic weight of Cu as 307.32 and 63.5, respectively, we can rationalize that the

most probable chemical composition of these monodispersed CuNCs to be $[\text{Cu}_{15}\text{GSH}_4 + 4 \text{ H}^+]$ (Figure 1b). Thus, in all probabilities, 15 Cu atoms constitute one NC as evidenced from the MALDI-TOF data. Further, our experimental results were strongly correlated with a theoretical approach based on the Jellium model²⁵ which also confirms the presence of 15 Cu atoms in the NCs.

The Jellium model²⁵ is a conventional theoretical approach for estimating atomic composition of the CuNCs according to the following equation:

$$E_{\text{em}} = E_{\text{Fermi}}/N^{0.33} \quad (1)$$

where E_{em} = emission energy of the nanoclusters (2.884 eV) at 430 nm, E_{Fermi} = Fermi energy of the Cu (7 eV), and N = number of metal atoms = 14.6.

Thus, from all this evidence, we conclusively assign our synthesized CuNCs to have a composition of $\text{Cu}_{15}\text{GSH}_4$.

3.2. Photophysical Properties. From the absorption spectra (Figure S4, Supporting Information), it is clear that the nature of absorption of the CuNCs is different as compared to GSH alone. Excitation-dependent emission spectra prove that the most pronounced excitation arises when $\lambda_{\text{ex}} = 340 \text{ nm}$ (Figure S5, Supporting Information), and when excited at this wavelength, the emission spectra (Figure 2a) of CuNCs exhibited intense blue luminescence (having a QY of ~6% with coumarin-153 as a reference²⁶) with the peak centered at 430 nm. In a seminal work Cau et. al have observed similar emission characteristics of CuNCs using tannic acid as a capping agent.²²

In order to have a better understanding of the excited-state properties of the CuNCs, we have performed picosecond time-resolved luminescence measurements. The lifetime of the NCs exhibited triexponential decay with an average value of 2.72 ns [1.39 (34.6%), 5.0 (42.5%), and 0.48 ns (22.9%)] (Figure 2b). Figure 3 compares the luminescence stability of the CuNCs, as

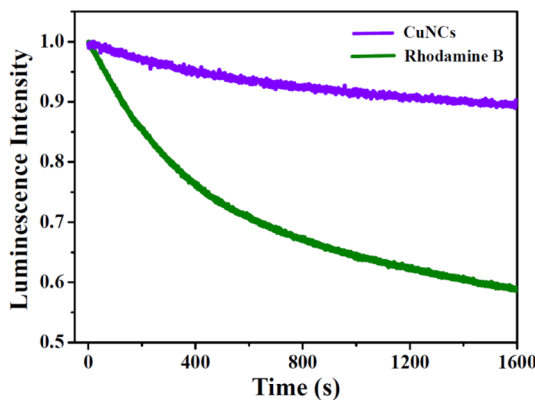


Figure 3. Simultaneous luminescence spectra of the CuNCs and rhodamine B as a function of time as marked in the figure.

a function of time, of the synthesized CuNCs to the otherwise photostable fluorescent dye rhodamine B. From this overlay, it is pretty clear that the luminescence of CuNCs remained almost constant under continuous irradiation, with a luminescence decrease rate of only $0.004\% \text{ s}^{-1}$ (compared to a rate of $0.028\% \text{ s}^{-1}$ for rhodamine B). Our synthesized CuNCs retain their stable luminescence properties under the variation of pH in the domain ranging from acidic to basic medium (Figure S6, Supporting Information). Further, we also observed almost constant luminescence intensity in the presence of

added salts like Na^+ , Ca^{2+} ions (Figure S7, Supporting Information). Besides having the properties as highlighted above, these CuNCs were stable even for over a month retaining almost all its spectroscopic properties (Figure S8, Supporting Information). Thus, all these optimum luminescence properties categorically establish that our stable CuNCs are capable and compatible for imaging cellular environments.

3.3. CuNCs as a Potential Bioimaging Probe. The excellent photostability makes our NCs potential candidates for bioimaging and biolabeling applications. To establish this fact, three different cancerous cell lines, Hela (malignant immortal cell line derived from cervical cancer), MDAMB-231 (human breast adenocarcinoma), and AS49 (human lung carcinoma) were chosen for the cell viability and uptake assays. We further aimed to identify the intracellular localization of our CuNCs in order to explore its biological function. To rule out that the CuNCs are detrimental for normal growth of the cells, we began with cellular viability test using different cell lines in culture. The cells were incubated with increasing concentrations ($1\text{--}200 \mu\text{M}$) of the CuNCs at 37°C . After different time intervals (2, 4, 6, 8, 15, and 36 h) post incubation, dead cells were counted using hemocytometer. We observed that, although at very high concentrations of the CuNCs ($75 \mu\text{M}$ to $200 \mu\text{M}$), cells died after 4 h of incubation, the compound does not, however, affect cell growth morphology at the lower concentrations up to $30 \mu\text{M}$ (Figure 4 and Table S1, Supporting Information).

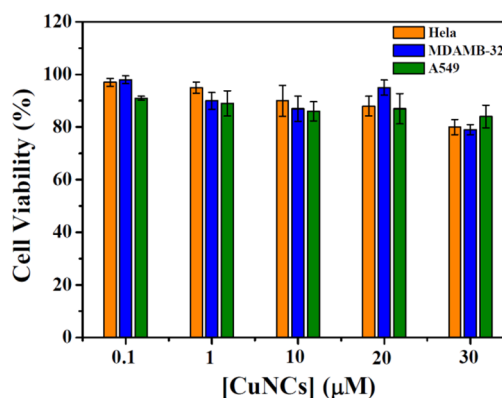


Figure 4. Viability of different cells after incubation with CuNCs in the concentrations range from 0 to $30 \mu\text{M}$. The error bars represents standard deviations based on three independent measurements.

Further, we investigated the intracellular localization of the compound using fluorescence microscopy. As revealed by laser scanning confocal microscopy (Figure 5), the compound primarily localizes to the region surrounding the nucleus, which might probably be the nuclear envelope of the cancerous cells.

As seen from Figure 5, clearly more CuNCs are distributed in the cytoplasm of AS49 cells as compared to the other cell lines. Hence, although CuNCs primarily localize to the nuclear membranes of the cells, the target factor may vary from cell line to cell line. Similar observations are also reported in the literature, where a single target molecule of interest shows very diverse types of localization in different types of cell lines.^{27,28} It has been reported that the subcellular localization of huntingtin, using antibody 1356, directed against the C-terminal end of the protein, shows cytoplasmic as well as a nuclear signal as revealed by the analysis in mouse embryonic fibroblasts

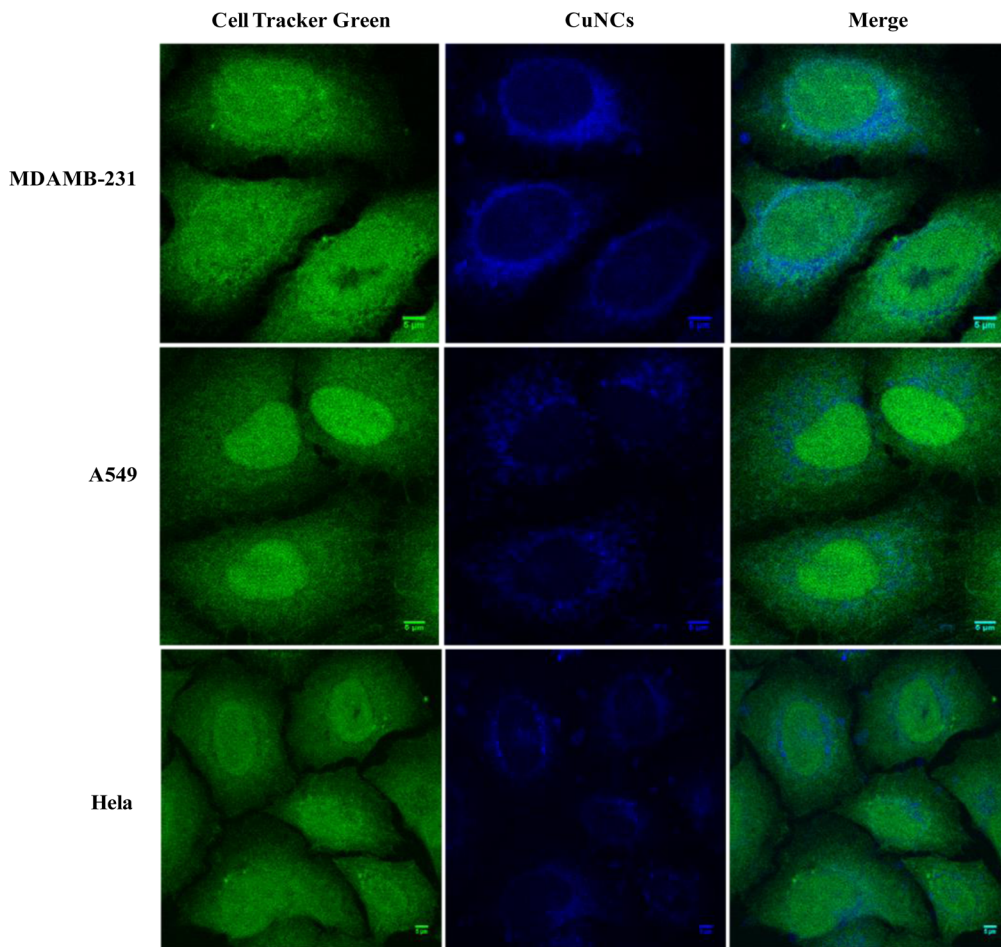


Figure 5. Subcellular localization of CuNCs: HeLa, MDAMB-231, and A549 cells were incubated with CuNCs for 12 h at 37 °C. The cells were labeled using CellTracker Green CMFDA (5-chloromethylfluorescein diacetate) before fixing in 4% paraformaldehyde. Images from the fixed cells were acquired using a laser scanning confocal microscope. The scale bar of the images represents 5 μ M in spatial size.

(MEFs), human skin fibroblasts, and mouse neuroblastoma cells.²⁷ Similarly, the intracellular localization of translationally controlled tumor protein (TCTP) was shown to localize in cytoplasm as well as nucleus in different cell lines.²⁸ The specificity comes from a target molecule which resides on a particular subcellular compartment. Most possibly the CuNCs bind to a component on the cytoplasmic face of nuclear envelop and thereby get localized to the region surrounding the nucleus. Presence of glutathione-recognizing motifs in a protein on the nuclear envelop could possibly make it an appropriate target for CuNCs. Hence, based on these results, we can conclude that our nonharmful and biocompatible CuNCs illustrate their excellent capability as a novel bioimaging and biolabeling probe which can be used to locate the cell in high-throughput screening as they are potential nuclear membrane markers (Figure 5). Since these NCs do not cause any damage to the cell growth, they can serve as novel agents to understand the dynamics of nuclear membrane in most cells during cell division/movement and also in locating the nucleus in tissue sections from normal and diseased cells.

3.4. Metal Ion Sensing Assay. For sensing studies, a series of aqueous solutions of different metal salts (Na^+ , Mg^{2+} , Ca^{2+} , K^+ , Mn^{2+} , Cr^{6+} , Fe^{3+} , Co^{2+} , Ni^{2+} , Cu^{2+} , Zn^{2+} , Hg^{2+} , and Pb^{2+}) were used and their concentration was initially kept at 10 nM, which was gradually increased up to 1 mM. On successive addition of metal ions to the solution of the CuNCs, the

changes in the luminescence properties were monitored. Among all the metal ions screened, only Fe^{3+} showed significant changes of luminescence (Figure 6).

On successive addition of Fe^{3+} ions to the CuNCs, we observed luminescence “turn off” behavior with almost 20% quenching in the presence of 10 μM Fe^{3+} ions. On further addition of Fe^{3+} ions to the CuNCs solution, the luminescence

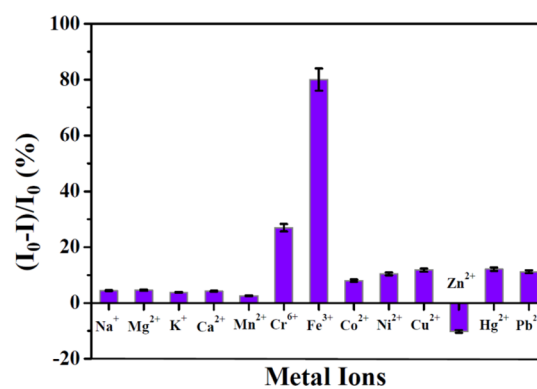


Figure 6. Histogram representing the extent of quenching of CuNCs in the presence 1 mM aqueous solution of different metals ions. I_0 and I are the luminescence intensities of CuNCs in the absence and presence of 1 mM metal ions, respectively.

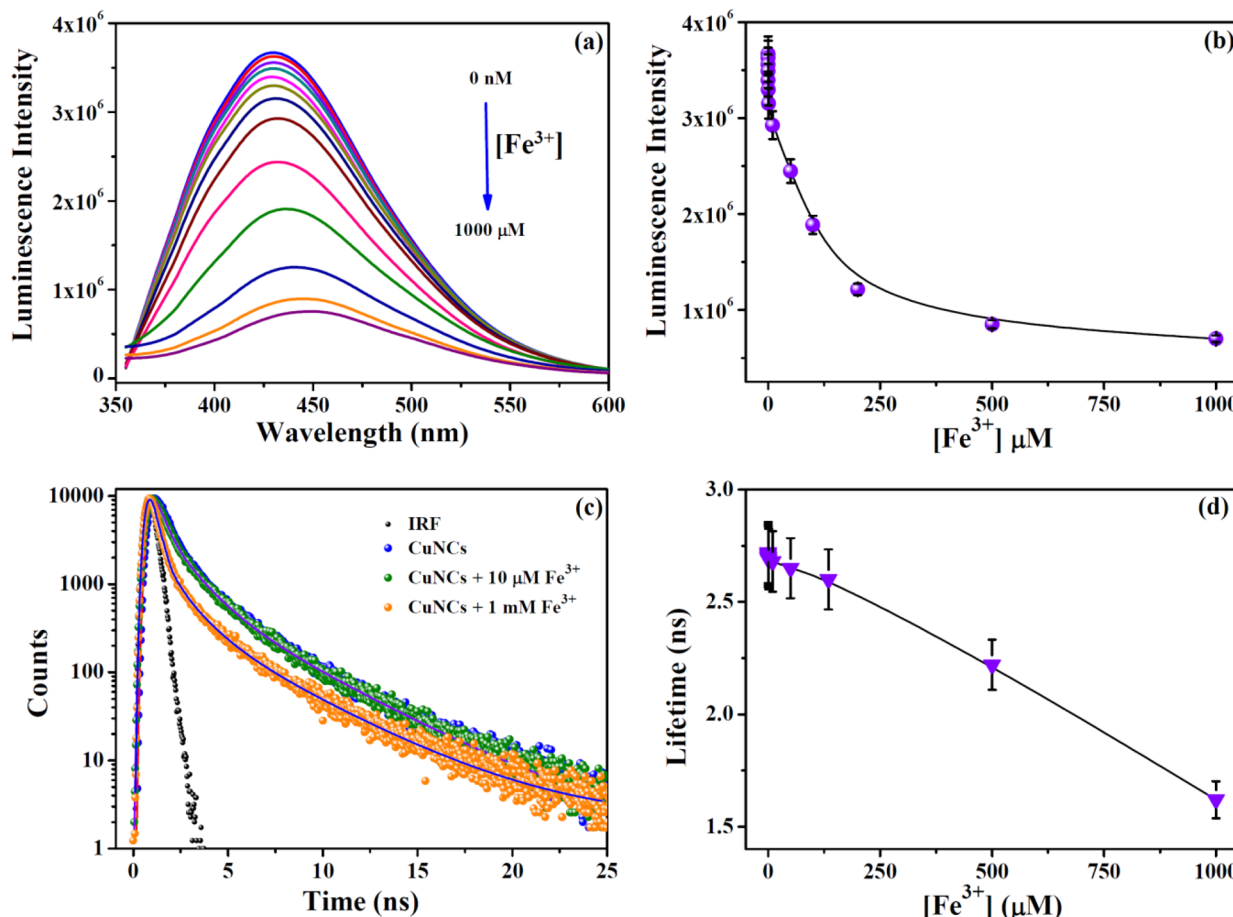


Figure 7. (a) Emission spectra of CuNCs in the presence of increasing concentrations of Fe^{3+} ions. (b) The variation in luminescence intensity of CuNCs in the presence Fe^{3+} ions. (c) Representative luminescence lifetime decay profiles of CuNCs in the presence of increasing concentrations of Fe^{3+} ions as marked in the figure. (d) Variation in the average luminescence lifetimes of CuNCs in the presence of different concentrations of Fe^{3+} ions.

intensity finally decreased up to 80% for 1 mM Fe^{3+} ions (Figure 7). Hence, our CuNCs assay showed very good potential as Fe^{3+} ions sensor with the limit of detection to be ~ 25 nM (please refer to the experimental section of the Supporting Information for details). To validate the exclusive and selective sensing capabilities of CuNCs, we have carried out luminescence experiments in the simultaneous presence of Fe^{3+} and other metal ions; even then only Fe^{3+} ions were sensed selectively. We have also studied the effect of anions keeping the cation fixed and found that, for both the cases, the luminescence intensities did not reveal any observable deviations in its emission characteristics, thereby establishing the fact that the performances of our sensor are not affected in any way. For unravelling the mechanistic pathways of the interaction of CuNCs with Fe^{3+} ions, Stern–Volmer analysis has been carried out. From the Stern–Volmer data, it is evident that the interaction is very strong and spontaneous (Figure S9 and Table S2, Supporting Information). For further clarification regarding the nature of interactive modes of CuNCs with Fe^{3+} ions, we have done time-resolved luminescence measurements (keeping experimental conditions similar to the steady-state protocols) which did not exhibit any significant changes in the lifetime for up to 10 μM Fe^{3+} ions (Figure S10, Supporting Information). However, on further addition of Fe^{3+} ions, a linear quenching behavior in the lifetime of CuNCs was evident (with 40% decrement for 1 mM Fe^{3+} ions). At lower

concentration of Fe^{3+} ions, the mechanism of quenching is primarily static in nature as a complex formation between the added Fe^{3+} ions with the CuNCs is envisaged. In this particular concentration regime, in all probabilities the Fe^{3+} ions bind on the surface of the CuNCs as evident from the quenching of steady-state luminescence and unaltered excited-state lifetimes. On further addition of the Fe^{3+} ions, its specific binding with CuNCs gets saturated and eventually interaction between them becomes dynamic in nature and simultaneously leads to weakening of the structural rigidity of the self-assembly of CuNCs. The mechanism of interaction is believed to be driven by electron transfer between CuNCs and Fe^{3+} ions.²² As stated earlier, besides serving as a stabilizing agent, the template GSH also provides a reducing environment. The outer electronic configuration of Fe^{3+} ion is $3d^54s^0$; these five half-filled d-orbitals make Fe^{3+} ions gain high positive charge density thereby inducing its strong electron-withdrawing character as compared to other metal ions.²⁹ Upon addition of Fe^{3+} ions, it withdraws electron from the surface of the CuNCs (furnished by the GSH template), and consequently, the structural compactness is reduced, which is responsible for the luminescence “turn off” characteristics of the CuNCs.^{22,30} Our time-resolved anisotropy data (Figure S11, Supporting Information) conclusively support this fact. The dynamic interaction behavior of Fe^{3+} ions (at higher concentration) with CuNCs is very well supported by the quenching of both the

steady-state and time-resolved luminescence. We have also observed ~27% luminescence quenching in the presence of 1 mM added Cr⁶⁺ ions, which may be attributed to the high positive charge density of Cr⁶⁺ ions, which weakens the structural rigidity of the NCs, although partially. Whereas in the case of Fe³⁺ ions, we observed ~80% quenching for the same concentration of the metal ion, and this is certainly proving its selective nature for Fe³⁺ ions. This specific interaction of Fe³⁺ ions with our synthesized CuNCs will enable us to delve into the nuances of the dynamical processes involved in iron-containing systems of biological relevance.

3.5. Quantitative Detection of Relative Percentage of Iron in Human Hemoglobin. To further establish the practical applicability of our CuNCs as sensors, we have carried out experiments using iron-containing biomacromolecule, Hb. For this Hb sensing assay, we added aqueous solution of Hb in the concentration range from 10 nM to 50 μM to the CuNCs (similar protocol as followed in other metal ion sensing) and the corresponding luminescent properties were recorded. In aqueous solution, iron is mainly present in Fe³⁺ state, and in Hb, the Fe²⁺ ions undergoes aerial oxidation to Fe³⁺ ions and results in the formation of methemoglobin. Higher concentrations of methemoglobin in human beings results in a disorder termed as methemoglobinemia, a clinical condition where Fe³⁺ ions have a decreased ability to bind oxygen. Consequently, the ability of the red blood cells to release oxygen to tissues is significantly reduced, which further results in tissue hypoxia and cyanosis.³¹ Detecting cyanosis at an early stage is crucial as, besides genetic reasons, it easily sets in because of many occupational hazards and exposure to chemicals.³² Clinically, cyanosis is detected when Fe³⁺ ions reaches a critical concentration of ~25%.³¹ The corresponding analyses of the Hb sensing behavior (whereby methemoglobin is actually sensed) also highlight the similar luminescence “turn off” characteristics as obtained from the Fe³⁺ ions sensing (Figure S12, Supporting Information). More interestingly, the relative percentage detection of iron was almost ~100% (please see the Supporting Information section for details). This sensitive detection ability of the CuNCs demonstrates the promising applicability of our methodology for the quantification of Fe³⁺ ions in blood samples and clinically detecting cyanosis at a very early stage.

4. CONCLUSIONS

In summary, we have been successful in establishing that the short peptide (GSH) templated CuNCs, which besides being rarely explored, are biocompatible and are highly photostable. MALDI-TOF methodology and calculations based on the Jellium model have been employed to estimate their chemical composition. Our cell-imaging studies reveal that CuNCs primarily localize in nuclear membranes of the different cancerous cells. The corresponding cell viability studies conclusively proved that our synthesized CuNCs are not detrimental for normal cell growth morphology in different cancerous cell lines and possess excellent potential to be used as a next-generation nontoxic and biomedical luminescent probe. The CuNCs also have immense potential as a metal ion sensor; they detected Fe³⁺ ions selectively at subnanomolar concentration in solution. We have also established that this aspect of Fe³⁺ ion sensing may help us in early detection of cyanosis as these NCs are competent to detect methemoglobin in human hemoglobin samples. All these superior characteristics of our blue-emitting versatile CuNCs highlight that this research field

opens a window for various interdisciplinary applications like photocatalysis and light-harvesting devices along with clinical/biomedical investigations.

■ ASSOCIATED CONTENT

■ Supporting Information

The Supporting Information is available free of charge on the ACS Publications website at DOI: 10.1021/acs.jpcc.5b08123.

Several spectroscopic analyses including UV-vis and luminescence of the CuNCs that show their morphological and photophysical properties (12 figures and 2 tables) (PDF)

■ AUTHOR INFORMATION

Corresponding Author

*E-mail: saptarshi@iiserb.ac.in.

Notes

The authors declare no competing financial interest.

■ ACKNOWLEDGMENTS

S.M. thanks the DST, Government of India, for project funds. N.K.D. and S.G. thank the UGC, Goverment of India, and A.P. thanks the IISER Bhopal for providing fellowships. S.M. also thanks Dr. Uttam Anand, University of Alberta, Dr. Somnath Mukherjee, AIIMS Bhubaneswar, and Dr. Joyanta Choudhury, IISER Bhopal for many stimulating discussions.

■ REFERENCES

- (1) Wei, W.; Lu, Y.; Chen, W.; Chen, S. One-Pot Synthesis, Photoluminescence, and Electrocatalytic Properties of Subnanometer-Sized Copper Clusters. *J. Am. Chem. Soc.* **2011**, *133*, 2060–2063.
- (2) Luo, Z.; Yuan, X.; Yu, Y.; Zhang, Q.; Leong, D. T.; Lee, J. Y.; Xie, J. From Aggregation-Induced Emission of Au(I)-Thiolate Complexes to Ultrabright Au(0)@Au(I)-Thiolate Core-Shell Nanoclusters. *J. Am. Chem. Soc.* **2012**, *134*, 16662–16670.
- (3) Anand, U.; Ghosh, S.; Mukherjee, S. Toggling Between Blue- and Red-Emitting Fluorescent Silver Nanoclusters. *J. Phys. Chem. Lett.* **2012**, *3*, 3605–3609.
- (4) Zheng, J.; Nicovich, P. R.; Dickson, R. M. Highly Fluorescent Noble-Metal Quantum Dots. *Annu. Rev. Phys. Chem.* **2007**, *58*, 409–413.
- (5) Derfus, A. M.; Chan, W. C. W.; Bhatia, S. N. Probing the Cytotoxicity of Semiconductor Quantum Dots. *Nano Lett.* **2004**, *4*, 11–18.
- (6) Enkin, N.; Sharon, E.; Golub, E.; Willner, I. Ag Nanocluster/DNA Hybrids: Functional Modules for the Detection of Nitroaromatic and RDX Explosives. *Nano Lett.* **2014**, *14*, 4918–4922.
- (7) Wen, Q.; Gu, Y.; Tang, L.-J.; Yu, R.-Q.; Jiang, J.-H. Peptide-Templated Gold Nanocluster Beacon as a Sensitive, Label Free Sensor for Protein Post-translational Modification Enzymes. *Anal. Chem.* **2013**, *85*, 11681–11685.
- (8) Xu, H.; Suslick, K. S. Sonochemical Synthesis of Highly Fluorescent Ag Nanoclusters. *ACS Nano* **2010**, *4*, 3209–3214.
- (9) Tanaka, S. I.; Miyazaki, J.; Tiwari, D. K.; Jin, T.; Inouye, Y. Fluorescent Platinum Nanoclusters: Synthesis, Purification, Characterization, and Application to Bioimaging. *Angew. Chem., Int. Ed.* **2011**, *50*, 431–435.
- (10) Stamplecoskie, K. G.; Kamat, P. V. Size-Dependent Excited State Behavior of Glutathione-Capped Gold Clusters and their Light-Harvesting Capacity. *J. Am. Chem. Soc.* **2014**, *136*, 11093–11099.
- (11) Ghosh, S.; Das, N. K.; Anand, U.; Mukherjee, S. Photostable Copper Nanoclusters: Compatible Förster Resonance Energy-Transfer Assays and a Nanothermometer. *J. Phys. Chem. Lett.* **2015**, *6*, 1293–1298.

- (12) Jia, X.; Yang, X.; Li, J.; Li, D.; Wang, D. Stable Cu Nanoclusters: From an Aggregation Induced Emission Mechanism to Biosensing and Catalytic Applications. *Chem. Commun.* **2014**, *50*, 237–239.
- (13) Cauzzi, D.; Pappacini, R.; Delferro, M.; Dini, F.; Di Natale, C.; Paolesse, R.; Bonacchi, S.; Montalti, M.; Zuccheroni, N.; Calvaresi, M.; Zerbetto, F.; Prodi, L. Temperature-Dependent Fluorescence of Cu₅ Metal Clusters: A Molecular Thermometer. *Angew. Chem., Int. Ed.* **2012**, *51*, 9662–9665.
- (14) Ghosh, R.; Goswami, U.; Ghosh, S. S.; Paul, A.; Chattopadhyay, A. Synergistic Anticancer Activity of Fluorescent Copper Nanoclusters and Cisplatin Delivered through a Hydrogel Nanocarrier. *ACS Appl. Mater. Interfaces* **2015**, *7*, 209–222.
- (15) Jia, X.; Li, J.; Wang, E. Cu Nanoclusters with Aggregation Induced Emission Enhancement. *Small* **2013**, *9*, 3873–3879.
- (16) Chen, Y.-S.; Kamat, P. V. Glutathione-Capped Gold Nanoclusters as Photosensitizers. Visible Light-Induced Hydrogen Generation in Neutral Water. *J. Am. Chem. Soc.* **2014**, *136*, 6075–6082.
- (17) Chen, F.; Gerion, D. Fluorescent CdSe/ZnS Nanocrystal-Peptide Conjugates for Long-term, Nontoxic Imaging and Nuclear Targeting in Living Cells. *Nano Lett.* **2004**, *4*, 1827–1832.
- (18) Chatteraj, S.; Bhattacharyya, K. Fluorescent Gold Nanocluster Inside a Live Breast Cell: Etching and Higher Uptake in Cancer Cell. *J. Phys. Chem. C* **2014**, *118*, 22339–22346.
- (19) Que, E. L.; Domaille, D. W.; Chang, C. J. Metals in Neurobiology: Probing their Chemistry and Biology with Molecular Imaging. *Chem. Rev.* **2008**, *108*, 1517–1549.
- (20) Ghosh, S.; Anand, U.; Mukherjee, S. Luminescent Silver Nanoclusters Acting as a Label Free Photoswitch in Metal Ion Sensing. *Anal. Chem.* **2014**, *86*, 3188–3194.
- (21) Weber, K. A.; Achenbach, L. A.; Coates, J. D. Microorganisms Pumping Iron: Anaerobic Microbial Iron Oxidation and Reduction. *Nat. Rev. Microbiol.* **2006**, *4*, 752–764.
- (22) Cao, H.; Chen, Z.; Zheng, H.; Huang, Y. Copper Nanoclusters as a Highly Sensitive and Selective Fluorescence Sensor for Ferric Ions in Serum and Living Cells by Imaging. *Biosens. Bioelectron.* **2014**, *62*, 189–195.
- (23) Dwivedi, A. K.; Saikia, G.; Iyer, P. K. Aqueous Polyfluorene Probe for the Detection and Estimation of Fe³⁺ and Inorganic Phosphate in Blood Serum. *J. Mater. Chem.* **2011**, *21*, 2502–2507.
- (24) Tajc, S. G.; Tolbert, B. S.; Basavappa, R.; Miller, B. L. Direct Determination of Thiol pKa by Isothermal Titration Microcalorimetry. *J. Am. Chem. Soc.* **2004**, *126*, 10508–10509.
- (25) Zheng, J.; Zhang, C.; Dickson, R. M. Highly Fluorescent, Water-Soluble, Size Tunable Gold Quantum Dots. *Phys. Rev. Lett.* **2004**, *93*, 077402.
- (26) Rurack, K.; Spieles, M. Fluorescence Quantum Yields of a Series of Red and Near-Infrared Dyes Emitting at 600–1000 nm. *Anal. Chem.* **2011**, *83*, 1232–1242.
- (27) De Rooij, K. E.; Dorsman, J. C.; Smoor, M. A.; Den Dunnen, J. T.; Van Ommen, G.-J. B. Subcellular Localization of the Huntington's Disease Gene Product in Cell Lines by Immunofluorescence and Biochemical Subcellular Fractionation. *Hum. Mol. Genet.* **1996**, *5*, 1093–1099.
- (28) Ma, Y.-P.; Zhu, W.-L. Cytoplasmic and Nuclear Localization of TCTP in Normal and Cancer Cells. *Biochem. Res. Int.* **2012**, *2012*, 871728.
- (29) Li, X. G.; Liao, Y.; Huang, M. R.; Strong, V.; Kaner, R. B. Ultra-Sensitive Chemosensors for Fe(III) and Explosives Based on Highly Fluorescent Oligofluoranthene. *Chem. Sci.* **2013**, *4*, 1970–1978.
- (30) Li, S.; Li, Y.; Cao, J.; Zhu, J.; Fan, L.; Li, X. Sulfur-Doped Graphene Quantum Dots as a Novel Fluorescent Probe for Highly Selective and Sensitive Detection of Fe³⁺. *Anal. Chem.* **2014**, *86*, 10201–10207.
- (31) Greer, J. P., Ed. *Wintrobe's Clinical Hematology*, 12th ed.; Lippincott Williams & Wilkins: Philadelphia, PA, 2009.
- (32) Linz, A. J.; Greenham, R. K.; Fallon, L. F., Jr. Methemoglobinemia: An Industrial Outbreak Among Rubber Molding Workers. *J. Occup. Environ. Med.* **2006**, *48*, 523–528.